Ferromagnetic resonance linewidth mechanisms in polycrystalline ferrites: Role of grain-to-grain and grain-boundary two-magnon scattering processes

Sangita S. Kalarickal,[1] Nan Mo,[1,*] Pavol Krivosik,[1,2] and Carl E. Patton[1]
[1]*Department of Physics, Colorado State University, Fort Collins, Colorado 80523, USA*
[2]*Slovak University of Technology, 81219 Bratislava, Slovakia*
(Received 12 December 2008; revised manuscript received 6 February 2009; published 30 March 2009)

The frequency dependence of the ferromagnetic resonance linewidth ΔH in polycrystalline hot isostatically pressed pure and Ca-Ge substituted yttrium iron garnet (YIG) spheres was measured between 1.95 and 6 GHz and analyzed. The linewidths for these ultradense ferrite materials are in the 5–40 and 5–25 Oe ranges for the pure and the substituted YIG samples, respectively. The ΔH vs frequency data show especially sharp Buffler peaks due to the band-edge crossover effect that is the signature for grain-to-grain (GG) two-magnon scattering (TMS) [C. R. Buffler, J. Appl. Phys. **30**, S172 (1959)]. Both the GG and recent grain-boundary (GB) TMS models were used to obtain quantitative fits to the data. The fits demonstrate the expected GG TMS contribution to the linewidth for frequencies above the Buffler peak. They also reveal two unexpected results: (1) a dominant GB TMS role for frequencies below the Buffler peak where the GG TMS linewidth contribution is essentially zero and (2) a significant GB TMS role for frequencies above the peak where the linewidth has generally been associated with GG processes only. In the high-frequency regime, the GB scattering term appears to explain about half of the overall linewidth.

DOI: 10.1103/PhysRevB.79.094427 PACS number(s): 75.50.Gg, 76.50.+g, 75.30.Ds, 75.40.Gb

I. INTRODUCTION

Despite many decades of study, the origins of microwave loss in polycrystalline magnetic materials remain a hot topic of research. There have been recent advances on several fronts, made possible in a large part by the availability of ultradense ferrite samples with near zero porosity and second phase.[1,2] The notable work of Nazarov *et al.*,[3] for example, was the first to demonstrate that ultradense polycrystalline ferrites can show close-to-theoretical linewidths based on grain-to-grain (GG) two-magnon scattering (TMS).

More recent work of Mo *et al.*,[4] in addition, has advanced the understanding of TMS relaxation processes in two ways. First, the application of clever metrology methods led to order-of-magnitude improvements in the accuracy of high-field effective linewidth measurements. This has led, in turn, to the discovery of a new role for hybrid electromagnetic-exchange spin waves and new grain-boundary (GB) two-magnon scattering in polycrystalline ferrites. Second, and in a completely different context, even more recent ferromagnetic resonance (FMR) linewidth measurements in nanocrystalline metallic magnetic films have demonstrated the crucial roles of both grain-to-grain and grain-boundary two-magnon scattering in microwave relaxation.[5,6]

This work returns to the problem of microwave relaxation in ultradense polycrystalline ferrites. The results from Ref. 3 have been extended to the low gigahertz regime and a comprehensive analysis of the full range of linewidth data over the characteristic Buffler peak[7] in a linewidth vs frequency data display format. This peak occurs for sphere samples when the FMR point moves above the top edge of the spin-wave band at low wave numbers. For the yttrium iron garnet (YIG) materials used here, this effect occurs at about 3 GHz. The analysis shows that both GG and GB processes play important roles in the structure of this Buffler peak.

The paper is organized as follows. Section II gives a brief qualitative description of two-magnon scattering processes in bulk ferrites and the qualitative origins of the Buffler peak. Section III elaborates sample properties, gives representative FMR profiles, and summarizes the overall linewidth vs frequency results. Qualitative connections to two-magnon scattering processes are also covered in this section. Section IV provides working equations for the quantitative analysis of the data. Section V presents theoretical fits to the data and makes specific connections to the linewidth contributions due to different scattering processes. Section VI gives a summary and conclusion.

II. VIGNETTE ON TWO-MAGNON SCATTERING IN BULK FERRITES

The early FMR data for ferrite materials generally showed larger linewidths than expected for intrinsic processes. Theoretical considerations by Clogston *et al.*[8] and Schloemann[9,10] showed two possible origins of these large linewidths: TMS processes and simple inhomogeneous line broadening. Inhomogeneity effects dominate when the corresponding local fields are large compared to the saturation induction $4\pi M_s$. Two-magnon scattering, while still based on inhomogeneities, is more subtle. TMS processes rely on small local effective-field spatial variations due to randomly oriented crystalline grain in anisotropic materials, dipole fields due to grain boundaries, second phase, pores, surface pits, magnetostriction, and so on. These field fluctuations lead to a coupling between the driven mode and available spin-wave modes at the same frequency. The coupling provides an additional channel for energy relaxation from the driven mode, first to the degenerate spin waves and eventually to the thermal bath. This is the essence of two-magnon scattering.

The first experimental signature of two-magnon scattering as a valid FMR relaxation process came from the seminal work of Buffler in 1959.[7] Schloemann's work,[9] noted above,

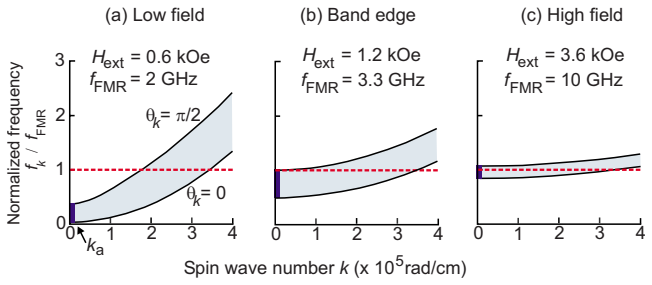

FIG. 1. (Color online) Schematic spin-wave band diagrams of spin-wave frequency f_k, normalized to the FMR f_{FMR}, as a function of the spin-wave number k for sphere shaped samples. Graphs (a)–(c) are for external applied static field (H_{ext}) values of 0.6, 1.2, and 3.6 kOe and the corresponding FMR frequency values, as indicated. Graph (b) corresponds to the band-edge crossover point at $f_{FMR}=f_X$. The curves are for yttrium iron garnet magnetic parameters. The curved lines show the band limits for spin-wave propagation angles (θ_k) relative to the field direction of zero and $\pi/2$ as indicated. The shaded regions indicate the full band. The horizontal dashed lines show the cut across the band at the FMR frequency for $f_k/f_{FMR}=1$. The arrow at $k_a \sim 1\times 10^4$ rad/cm and narrow vertical shaded regions for $k<k_a$ denote the region of strong two-magnon grain-to-grain scattering for a nominal grain size of 10 μm.

had pointed out a peculiar spin-wave band effect for sphere shaped samples. As one increases the applied field, there is a point at which the FMR frequency crosses the top edge of the low wave-number limit of the spin-wave band. More specifically, the FMR point starts above this limit at low field and moves into the band only at high field. For YIG spheres, as an example, this band-edge crossover point occurs in the 3.5 GHz range, depending on the actual saturation induction of the material.

Even today, many FMR experts do not know about this basic effect, even though it provides the historical experimental key to two-magnon scattering relaxation. One possible reason is that the predominant FMR work in recent years has been for thin films. This band-edge crossover effect occurs only for spheres and not for any of the other basic geometries of interest.

The experimental manifestation of this effect is an abrupt increase in the linewidth as the FMR frequency moves through the crossover frequency, taken here as f_X. This is then followed by a slow decrease in the linewidth at higher frequencies. This is a purely geometric effect. It occurs for spheres but not for other sample shapes. Buffler[7] was the first to observe this effect experimentally. This direct early experimental evidence for TMS processes provided the key data that pointed the way to further theory and experiments on anisotropy, porosity, and surface pit TMS processes.[11] As noted in Sec. I, new results continue to emerge. Mo *et al.*[6] have shown, for example, that grain-boundary TMS processes related to very short-wavelength spin waves must be added to the above list of interactions for a complete picture of this important mechanism.

Figure 1 illustrates the band-edge crossover effect described above. The (a)–(c) graphs show spin-wave band diagrams of normalized spin-wave frequency vs wave number k for three different fields for sphere shaped YIG samples, as indicated. Graph (b) corresponds to the FMR band-edge crossover. The specific field/frequency operating points were chosen to demonstrate this effect. The dashed horizontal line shows the degenerate mode cut across the bands at the FMR frequency for these three cases. The vertical shaded region across the low k edge of the band for $k<k_a=1\times 10^4$ rad/cm accentuates those modes that can give a strong GG TMS contribution for YIG grain sizes in the 10 μm range. The connection between k_a, grain size, and TMS processes will be elaborated shortly.

Figure 1 is intended to convey two main points. First, as one increases the external field, the well-known upward shift in spin-wave band and the FMR frequency is accompanied by a crossover of the FMR frequency from outside the low k part of the band at low field to completely inside the band at high field. The crossover frequency f_X is equal to $(2/3)(|\gamma|/2\pi)4\pi M_s$, where γ denotes the electron gyromagnetic ratio. With $4\pi M_s$ taken at the nominal YIG value of 1750 G and $|\gamma|/2\pi$ taken at the nominal free-electron value of 2.8 GHz/kG, this crossover effect occurs at about 3.3 GHz. The specific diagrams in Fig. 1 have been selected to underscore this basic effect. It is a little known effect, even though it was crucial to the initial realization of the role of TMS processes in microwave ferrite relaxation.

The second point concerns the interplay between the actual coupling to the degenerate modes and the crossover effect that leads to the TMS signature in the linewidth vs frequency profile discovered by Buffler.[7] In this context, the key is in the shaded vertical strip of modes at the extreme low k side for each of the spin-wave band diagrams in Fig. 1. This strip corresponds to the modes that are strongly coupled to the FMR mode for coarse grain ferrites. Here, "coarse grain" is taken to denote grain sizes in the range of tens of micrometers that are typical for polycrystalline ferrites made by standard sintering or hot pressing methods.

Generally, two-magnon scattering has a strong coupling between the driven FMR mode for $k\approx 0$ to degenerate spin-wave modes with $k<k_a\approx 1/a$ or so, where a is the grain size. For $a\sim 10$ μm, one has $k_a\approx 10^4$ rad/cm. One can see that as the field is increased and the FMR frequency moves from above the band-edge point to inside the band, the low k modes available for strong scattering come into play quite abruptly. The fact that the density of states for the degenerate spin-wave modes is also quite large at the top edge of the spin-wave band leads to a pronounced peak in the linewidth as one moves through the crossover frequency. The quantitative connection between the linewidth vs frequency data and the TMS analysis for GG scattering will be covered in Sec. IV. Additionally, the results will also reveal another effect, namely, a nonzero GB scattering to high k spin-wave modes. This effect shows up most clearly for frequencies in the band regime of graph (a) in Fig. 1. One can see that for GG scattering alone, the TMS linewidth in this regime is zero because there are no degenerate low k modes.

III. SAMPLES AND MEASUREMENTS

The YIG samples were made by standard hot isostatic pressing (Hipping) ceramic methods. Nazarov *et al.*[3] have

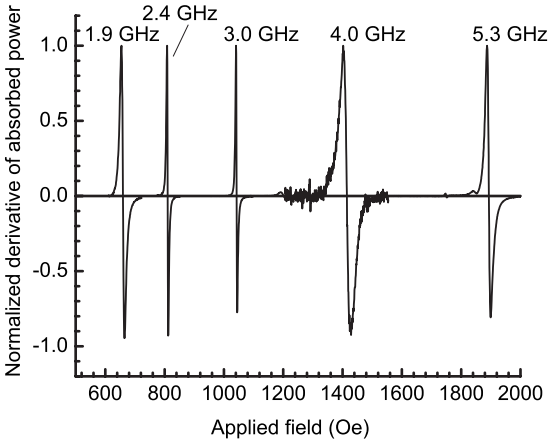

FIG. 2. Normalized FMR absorption derivative vs field profiles for the hipped YIG sphere at selected FMR pump frequencies, as indicated.

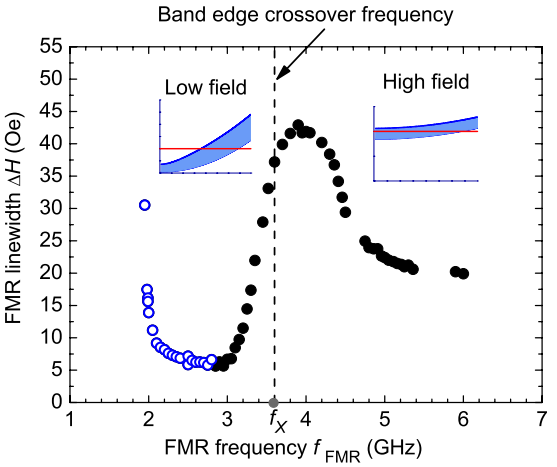

FIG. 3. (Color online) FMR linewidth ΔH as a function of the FMR frequency f_{FMR} for the hipped YIG sphere. The open blue symbols show data for the low-field regime for which the sample is not saturated. The vertical dashed line marks the calculated band-edge crossover frequency f_X. The insets show schematic spin-wave frequency vs wave-number diagrams for the low field below crossover ($f<f_X$) and high field above crossover $f>f_X$ regimes.

provided the fabrication details. These authors also provided X-band FMR linewidth data that establish the density of the materials to be near theoretical. The residual porosity was less than 1% and the half power 10 GHz FMR linewidth was 13 Oe. The average grain size was 8 μm. Spheres were fabricated from the interior regions of the hipped blocks to avoid possible problems with oxygen deficient surface regions. A similar procedure was also applied to Ca-Ge substituted YIG. The specific results in this chapter, shown for nominal 2 mm diameter spheres, confirm the nearly complete elimination of porosity for the hipped materials.

The FMR profiles were measured at frequencies between 1.95 and 6 GHz with a broadband strip transmission line FMR spectrometer described in Ref. 12. Figure 2 shows representative data. The graph shows a sequence of profiles of the FMR absorption derivative vs static external field H_{ext} for selected frequencies, as indicated. One sees the expected shift in the FMR fields with increasing frequency. Note that the profile is somewhat narrow at 1.9 GHz, becomes very narrow at 3 GHz, broadens substantially at 4.0 GHz, and then appears to narrow somewhat at 5.3 GHz. The behavior from 3 to 5.3 GHz is a direct consequence of the band-edge crossover GG TMS effect from Sec. II. The substantial jump in linewidth from 3 to 4 GHz is a direct result of this crossover. The falloff from 4 to 5.3 GHz is due to a gradual drop in the available degenerate spin-wave states for scattering. The relatively broad line at 1.9 GHz is due to the unsaturated state of the sample at these fields.

Data of the sort shown in Fig. 2 were also used to establish the gyromagnetic ratio γ. The FMR frequency f_{FMR} for sphere shaped samples is equal to $(|\gamma|/2\pi)H$. The data on FMR frequency vs field yielded a $|\gamma|/2\pi$ value of 2.765 MHz/Oe. This paper will use Gaussian units for the working equations for the data analysis, as needed, and for the theoretical development. Note also that the f notation will denote frequency in hertz or related units. In the theoretical discussions to follow, it will also be appropriate to bring in the usual ω notation for angular frequency in rad/s.

Linewidth values were obtained from FMR derivative profiles similar to those shown in Fig. 2 but for a fine grid of frequency points from 2 to 6 GHz. For each profile, the half power field swept linewidth ΔH was taken as the difference in field values at the extrema of the derivative profile multiplied by $\sqrt{3}$. This connection is strictly applicable to Lorentzian absorption profiles. Integrated absorption profiles were, in fact, near Lorentzian.

Figure 3 shows representative ΔH vs f_{FMR} results. These particular data, as in Fig. 2, are for the hipped YIG sphere. The main portion of the data is shown by solid symbols. These data will be the focus of the two-magnon analysis to follow. The portions of the data for $f_{\mathrm{FMR}}<3$ GHz or so are shown by blue open circles. These data show a gradual upturn below 3 GHz and a more rapid increase below about 2.2 GHz. This response is related to demagnetization and low-field loss effects and is not of direct interest here. The vertical dashed line at $f_{\mathrm{FMR}}\approx 3.6$ GHz marks the band-edge crossover frequency. This point is shifted from the 3.3 GHz value shown in Fig. 1 because of the larger nominal $4\pi M_s$ value of 1950 G for the hipped YIG material, as obtained from fits to be considered shortly. The schematic low-field and high-field region spin-wave band diagrams for the regions below and above the crossover point track the (a) and (c) diagrams from Fig. 1.

The solid circle data in Fig. 3 demonstrate the two-magnon band-edge crossover effect discussed in Sec. II. There is a rapid increase in linewidth as one approaches the crossover frequency from below, followed by a distinct peak and a gradual leveling off at high frequency. It is notable that there is sizable linewidth increase even for frequencies below the crossover frequency. The coarse grain scattering scenario from Sec. II and the exclusive two-magnon coupling to extremely low k modes alone would give a sharp cutoff at the crossover frequency f_X rather than the response shown by the data. As will be discussed shortly, the two-magnon linewidth "leakage" into the frequency regime below f_X is a direct result of grain-boundary TMS processes. It also turns out that

GB scattering also plays a significant role in the frequency regime above crossover. This is alluded to in the last part of the discussion of Fig. 1 at the end of Sec. II. These points will be made quantitative in Secs. IV and V.

IV. TWO-MAGNON SCATTERING RELAXATION AND LINEWIDTH CONNECTIONS

As noted in Sec. II, there is extensive literature on the two-magnon scattering relaxation theory in magnetic systems in general.[8–11,13–15] Mo *et al.*[4] cast the general two-magnon scattering relaxation rate in the form

$$\eta_{\mathrm{TMS}} = \frac{\omega_M^2}{8\pi^3}\int_{\mathbf{k}\ \mathrm{space}} \delta(\omega-\omega_k)C(\mathbf{k})\Lambda(\mathbf{k},\omega)d\mathbf{k}. \tag{1}$$

The parameter $\omega_M=|\gamma|4\pi M_s$ expresses the saturation induction in frequency units. The delta function $\delta(\omega-\omega_k)$ constrains the scattering to degenerate spin-wave modes with a frequency ω_k equal to the pump frequency ω. The $C(\mathbf{k})$ factor defines the coupling strength between the uniform mode and particular degenerate spin-wave modes at some wave vector $\mathbf{k}$. The $\Lambda(\mathbf{k},\omega)$ factor accounts for the ellipticity of the spin-wave mode. For sphere shaped samples, the connection between η_{TMS} and ΔH amounts to a simple conversion, according to $\Delta H=2\eta_{\mathrm{TMS}}/|\gamma|$.

As discussed in earlier sections, two distinct TMS processes turn out to be important for polycrystalline ferrites, one related to GG scattering and the other to GB scattering. These processes can be taken to occur in parallel. In order to deal with the differences in the k dependences of the coupling terms for the two processes, it proves useful to write Eq. (1) in a slightly different form. Keep in mind that for GG scattering, it is the grain size a that controls the scattering and the coupling is to low wave-number modes with $k<k_a$ alone. Recall the discussion related to Fig. 1 and coarse grain scattering. For GB scattering, it is the much narrower submicron size grain boundary that controls the scattering. This process is definitely not coarse grain scattering but extends out to much larger k values.

A useful starting point for the separation of the different k dependences for GG and GB scattering is to recast the formal $\mathbf{k}$-space integral in Eq. (1) in terms of the specific integrals over wave number k and the polar and azimuthal spin-wave propagation angles θ_k and ϕ_k, respectively,

$$\eta_{\mathrm{TMS}} = \frac{\omega_M^2}{8\pi^3}\int_0^\infty dk\int_0^1 d\cos\theta_k[F(\mathbf{k})\Lambda(\mathbf{k},\omega)\delta(\omega-\omega_k)]. \tag{2}$$

The function $F(\mathbf{k})=4\pi k^2 C(\mathbf{k})$ folds in the numerical 4π factor from the angular integrals and the explicit k^2 factor from the k integral into the new form of the coupling. As the discussion below will demonstrate, the $F(\mathbf{k})$ form makes it possible to gain an intuitive understanding of the GG and GB contributions to the scattering.

First consider the working equations for GG scattering. In this case, one can write $F(\mathbf{k})$ in the form

$$F_{\mathrm{GG}}(\mathbf{k}) = F_{\mathrm{GG}}(k) = \frac{8\pi^4}{105}\left(\frac{H_A}{4\pi M_s}\right)^2 g(k). \tag{3}$$

The $g(k)$ function is used here to separate out the k-dependent part of the degenerate spin-wave coupling for GG scattering. This factor is taken in the form first used by Schloemann[9] and recently rederived by Hamiltonian methods by Krivosik *et al.* in Ref. 14,

$$g(k) = \frac{4}{\pi}\frac{k^2a^3}{(1+k^2a^2)^2}. \tag{4}$$

In the above, H_A denotes an effective cubic anisotropy field $2K_1/M_s$, where K_1 is the first-order cubic magnetocrystalline anisotropy energy constant. In the qualitative discussion above, a was taken as the grain size. In a more general sense, a may be taken as a mean inhomogeneity size. One can see that the $g(k)$ function peaks at $k=k_a=1/a$. Recall, however, that the k^2 factor in the numerator derives from the same factor in the k-space differential volume $4\pi k^2 dk$. Without this factor, the $g(k)$ corresponds to the Fourier transform of a fluctuating field with a correlation length equal to the mean grain size.

The spin-wave ellipticity factor for GG scattering, labeled here as $\Lambda_{\mathrm{GG}}(\mathbf{k},\omega)$, was also developed first by Schloemann in Ref. 9 and is written here as

$$\Lambda_{\mathrm{GG}}(\mathbf{k},\omega) = 1 + 19\frac{A(\mathbf{k},H)}{\omega}, \tag{5}$$

where

$$A(\mathbf{k},H) = |\gamma|H_i + |\gamma|Dk^2 + |\gamma|2\pi M_S \sin^2\theta_k. \tag{6}$$

The internal field H_i in Eq. (6) is equal to $H-(4\pi M_S/3)$ for sphere shaped samples. The D parameter takes exchange into account. The nominal D value for YIG materials is 5.2×10^{-9} Oe cm^2.[4] The numerical factors in Eqs. (3) and (5) follow the Schloemann form. They are a result of a systematic averaging over the randomly oriented cubic crystallites for the YIG system. Further details on the averaging mechanics are given by McMichael and Krivosik in Ref. 13.

For GB scattering, the $F(\mathbf{k})$ and $\Lambda(\mathbf{k},\omega)$ functions take a somewhat different form. The full theory is summarized in Refs. 4 and 6 and developed in detail in Ref. 15. The coupling and polarization terms are different from those for the grain-grain anisotropy based scattering. The formulas given below follow the nomenclature in Ref. 4. The $F(\mathbf{k})$ for GB scattering now takes the form

$$F_{\mathrm{GB}}(\mathbf{k}) = F_{\mathrm{GB}}(k) = 12\pi^4 l_{\mathrm{gb}}^2 k^2 g(k). \tag{7}$$

Following Ref. 4, l_{gb} denotes an effective grain-boundary thickness parameter. From physical considerations, l_{gb} scales with the ratio of surface anisotropy energy to the magnetostatic self-energy and is on order of tens of nanometers for polycrystalline ferrites. Fits to the data in Sec. V will yield nominal values of 9 nm for the pure YIG and 16 nm for the Ca-Ge substituted YIG samples. Note the additional k^2 factor in the GB coupling. With this modification, the k dependence of the scattering defined through $k^2 f(k)$ sees major modifications. Now the scattering is essentially zero for $k \ll k_a$, begins

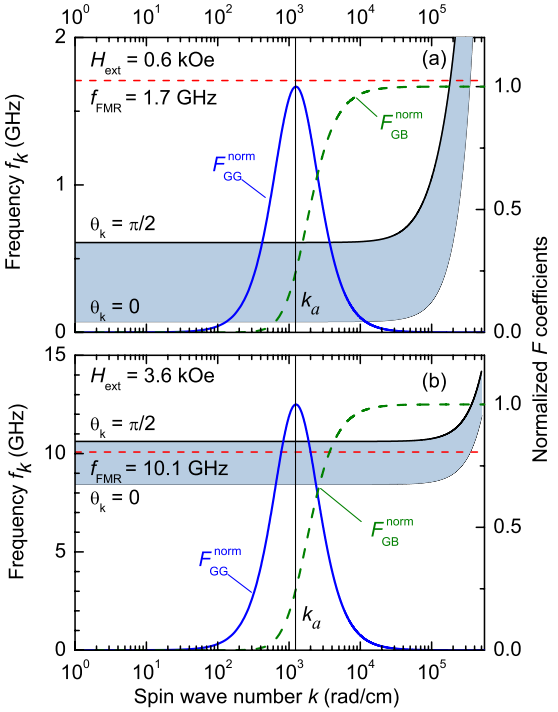

FIG. 4. (Color online) Each graph shows (i) spin-wave frequency f_k vs wave number k for a sphere shaped yttrium iron garnet sample with material parameters that match the experiment and (ii) the normalized two-magnon scattering coupling coefficient F^{norm} vs k for GG and GB TMSs, as indicated. The curves in (a) and (b) were obtained with external field H_{ext} values of 0.6 and 3.6 kOe, respectively. The spin-wave band nomenclature and labels are the same as for Fig. 1. The solid vertical line at $k=k_a=1/a=1.25\times10^3$ rad/cm, where a is the nominal grain size, marks the transition k value for both TMS processes.

to grow for $k\approx k_a$, and levels off to some maximum value for $k\gg k_a$. This is precisely the response expected for GB scattering. One can now have strong coupling to very short-wavelength spin waves in the extremely high k part of the spin-wave manifold.

Also following Ref. 4, the $\Lambda(\mathbf{k},\omega)$ spin-wave polarization term for GB scattering is now written as

$$\Lambda_{\text{GB}}(\mathbf{k},\omega) = 1 + \frac{A(\mathbf{k},H)}{\omega}. \tag{8}$$

The different numerical factors in Eqs. (6) and (8) arise from the different symmetries in the GG and GB scattering problems. As noted above, GG scattering involves an averaging over the grains in the three-dimensional (3D) system. For GB scattering, in contrast, one is dealing with an interface effect that is treated in a simplified two-dimensional (2D) model.[15]

Figure 4 shows the same bulk spin-wave band diagrams of frequency f_k vs wave number k as given in graphs (a) and (c) of Fig. 1, except that the k axis is given in logarithmic scale. Also as in Fig. 1, horizontal dashed red lines are used to show k range of the degenerate mode at the indicated FMR frequency in each case. The solid blue and dashed green curves in both graphs show plots of the $F(k)$ functions developed above for GG and GB scatterings, respectively. The curves are normalized to maximum values and denoted as $F^{\text{norm}}(k)$. Recall that the peak GG coupling occurs for $k=k_a=1/a$. The GB coupling shows no peak but simply levels off at its maximum value at very high k values.

The overall point of Fig. 4 is to demonstrate the very different coupling conditions for fields below the band edge, as in (a), and fields above the band edge, as in (b). For the below-the-band-edge situation in (a), one can see that the degenerate mode line cuts the spin-wave band in the range of very high k values for which the GB coupling is strong and that there are no degenerate low k modes. This means that the two-magnon processes are limited to GB scattering. As will be shown shortly, GB scattering turns out to provide a reasonable quantitative model for the observed linewidth tail for frequencies below the band-edge crossover frequency f_X.

Contrast this with the situation in Fig. 4(b). Here one can see that the degenerate mode line cuts the spin-wave band over the full range of wave-number k values from the low limit at $k\approx0$ out to the very high values at the edge of the spin-wave band for $k\approx10^5-10^6$ rad/cm. These degenerate modes now span regions of k space for which the $F(k)$ functions for *both* GG and GB scatterings indicate strong coupling. The quantitative fits of the theory to the data given below will show that both processes contribute substantially to the two-magnon linewidth for frequencies above the band-edge crossover frequency f_X.

V. LINEWIDTH ANALYSIS

Graphs (a) and (b) in Fig. 5 show the full ensemble of linewidth vs frequency data for both the pure YIG and substituted YIG samples, respectively. The open circles in (a) show the same data as in Fig. 3. The solid circles show extended frequency data from Ref. 3. The error bars for all data points are in the range of ±0.5 Oe. The panels also show theoretical fits based on a simple model of GG and GB TMS processes that operate in parallel. The fits do not include either a Landau-Lifshitz linewidth term or inhomogeneity broadening effects. The various curves show computed results for GG scattering, GB scattering, and the sum of these two processes, as indicated. The theoretical curves were obtained for a common grain size a of 8 μm, and with $4\pi M_s$, H_A, l_{gb}, and $|\gamma|/2\pi$ values of 1952 G, 40 Oe, 9 nm, and 2.765 MHz/Oe, respectively, for the pure YIG and 990 G, 20 Oe, 16.2 nm, and 2.76 MHz/Oe, respectively, for the substituted YIG. These material parameters are consistent with the ferrite literature.[16,17] The critical fit parameters were H_A and l_{gb}. Following Ref. 4, an effective grain-boundary thickness parameter l_{gb} in the nanometer range is also reasonable for the hipped ferrite microstructure.

Both graphs show very prominent Buffler peaks. In line with the extended discussion in Sec. III, these peaks provide the basic signature of GG scattering. The prominence of the Buffler peaks is due to the use of hipped samples with near theoretical density. Porosity effects in the original Buffler samples resulted in significantly larger linewidths and a

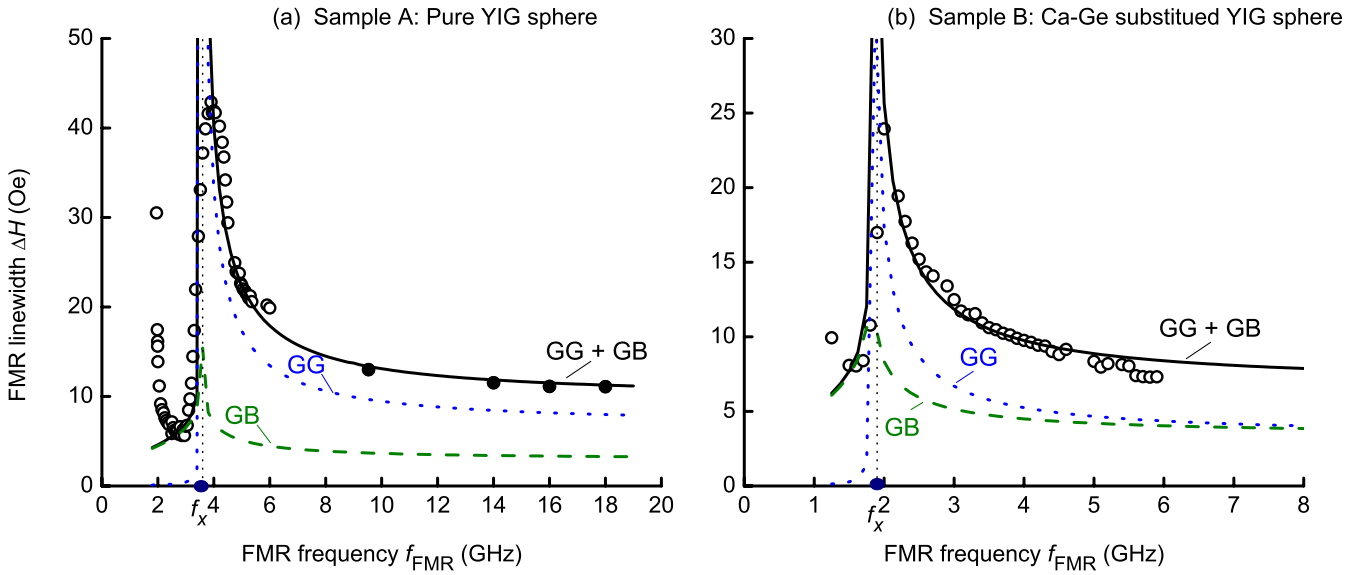

FIG. 5. (Color online) Graphs (a) and (b) show the FMR linewidth ΔH as a function of the FMR frequency f_{FMR} for sphere shaped samples of hipped YIG and Ca-Ge substituted YIG, respectively. The open circles show data from the broadband strip transmission line measurements. The solid circles in (a) show data on the same sample from Nazarov *et al.* (Ref. 3). The dashed and dotted curves show fitted ΔH vs f_{FMR} results from model calculations for GB and GG two-magnon scattering processes, respectively. The solid curves show the sum of the GB and GG results.

broader peak. Overall, the linewidths in (b) for sample B are even lower than those in (a) because of the use of Ca-Ge substituted YIG materials with a lower anisotropy. The GG based two-magnon scattering scales with the anisotropy.[16,18]

The physical origins of the linewidth vs frequency response manifested by the low-frequency data in (a) were discussed in connection with Fig. 3. From Fig. 5, one sees that both samples show essentially the same response. Each data set shows (1) a rapid increase in linewidth at very low frequencies due to sample demagnetization, (2) a local minimum with a nonzero linewidth at frequencies just below the Buffler peak, (3) a rapid increase that forms the Buffler peak as one moves through the band-edge crossover, and (4) a gradual decrease in linewidth as one moves to frequencies well above the Buffler peak. These effects occur for somewhat lower frequencies in (b) due to the reduced magnetization for the Ca-Ge-YIG.

The new points to be considered here, relative to Fig. 3, concern the actual fits to the data from the combined GG and GB TMS models. These fits tell the quantitative story of the TMS processes outlined in general terms in Secs. III and IV. The fits demonstrate three points. First, it is clear that one can realize a remarkably good fit to the data for two different materials based on TMS processes. The fact that the theoretical curves show a divergence at the band-edge crossover frequency is of no consequence here. This divergence is due to the neglect of the nonzero relaxation rate for the product spin waves from the TMS processes. Schloemann[9] has shown that the inclusion of a nonzero spin-wave linewidth in TMS calculations eliminates such divergences. One obtains, thereby, theoretical curves that match effective linewidth data quite nicely, for example.[17]

Second, the GB TMS linewidth fits for the frequency region just below the Buffler peak band confirm the expectation from Sec. IV that grain-boundary scattering processes must play a role in this region. In fact, the theoretical response also matches this portion of the data quite nicely.

The third point comprises a somewhat unexpected result. The realization of data over a wide range of frequencies on both sides of the Buffler peak, in combination with calculations based on a two component GG/GB TMS process, shows that both processes make significant contributions to the linewidth. The fits in Ref. 3 were done for GG scattering alone and appeared to match the data. The problem in this reference, however, was in the availability of limited high-frequency data only and no experimental points close to or below the Buffler peak. In the present work, it is these low-frequency data points that provide the clue to the role of GB scattering. Once the required GB scattering parameters are included to fit the data for $f<f_X$, a necessary GB contribution propagates into the $f>f_X$ frequency regime. The fits show that in the $f>f_X$ region, one has roughly equal GG and GB two-magnon scattering contributions to the linewidth.

With two-magnon processes properly taken into account, it is entirely reasonable to ignore any possible intrinsic linewidth terms in doing the fits shown in Fig. 5. Effective linewidth measurements have shown that such contributions are below 1 Oe over the frequency range shown here.[19]

VI. SUMMARY AND CONCLUSION

The early linewidth results for polycrystalline ferrites in the region of the Buffler peak provided the initial evidence for the role of two-magnon scattering relaxation in ferromagnetic resonance. These classic results have been now extended and made quantitative, and several aspects of TMS relaxation in polycrystalline ferrites have been revealed. The data on ultradense pure and substituted YIG materials with

nominal 10 μm grain sizes show an especially sharp Buffler peak that derives from the band-edge crossover effect initially reported in Ref. 7. Due in part to recent new developments in two-magnon relaxation models for both GG anisotropy scattering and GB scattering, it has been possible to obtain quantitative TMS fits to the data. These fits demonstrate the expected role of GG scattering in the relaxation, just as suggested by Buffler.[7] The fits also reveal the somewhat unexpected role of GB scattering as a contributor to the TMS linewidth in polycrystalline ferrites. (1) It is found that GB scattering plays a role in the frequency regime below the Buffler peak where simple two-magnon low k scattering models give no TMS contribution. The nominal GB TMS linewidth in this regime is about 5 Oe. (2) It is also found that GB scattering contributes about half of the overall TMS linewidth in the frequency regime above the peak where GG scattering was previously thought to be dominant.

ACKNOWLEDGMENTS

This work was sponsored in part by the Office of Naval Research under Grants No. N00014-07-1-0597 and No. N00014-08-1-1050 (subgrant from Virginia Commonwealth University), the U.S. Army Research Office under Grant No. W911NF-04-1-0247 (MURI), the Information Storage Industry Consortium extremely high-density recording program, and the Seagate Technology. The hipped pure YIG sample was kindly provided through a collaboration with G. M. Argentina (Pacific Ceramics, Inc.) and J. J. Green and H. J. Van Hook (private consultants, Lexington, Massachusetts). The hipped substituted YIG sample was kindly provided by TCI Ceramics, Bethlehem, Pennsylvania.

*Present address: Communications and Industrial Solutions, Tyco Electronics, Reno, Nevada 89521, USA.

[1] H. J. Van Hook and C. B. Willingham, Adv. Ceram. **15**, 1637 (1984).
[2] H. V. Atkinson and S. Davies, Metall. Mater. Trans. A **31**, 2981 (2000).
[3] A. V. Nazarov, D. Menard, J. J. Green, C. E. Patton, G. M. Argentina, and H. J. Van Hook, J. Appl. Phys. **94**, 7227 (2003).
[4] N. Mo, J. J. Green, P. Krivosik, and C. E. Patton, J. Appl. Phys. **101**, 023914 (2007).
[5] S. S. Kalarickal, P. Krivosik, J. Das, K. S. Kim, and C. E. Patton, Phys. Rev. B **77**, 054427 (2008).
[6] N. Mo, J. Hohlfeld, M. u. Islam, C. S. Brown, E. Girt, P. Krivosik, W. Tong, A. Rebei, and C. E. Patton, Appl. Phys. Lett. **92**, 022506 (2008).
[7] C. R. Buffler, J. Appl. Phys. **30**, S172 (1959).
[8] A. M. Clogston, H. Suhl, L. R. Walker, and P. W. Anderson, J. Phys. Chem. Solids **1**, 129 (1956).
[9] E. Schlömann, J. Phys. Chem. Solids **6**, 242 (1958).
[10] E. Schlömann, Phys. Rev. **182**, 632 (1969).
[11] M. Sparks, *Ferromagnetic Relaxation Theory* (McGraw-Hill, New York, 1964).
[12] S. S. Kalarickal, P. Krivosik, M. Wu, C. E. Patton, M. L. Schneider, P. Kabos, T. J. Silva, and J. P. Nibarger, J. Appl. Phys. **99**, 093909 (2006).
[13] R. D. McMichael and P. Krivosik, IEEE Trans. Magn. **40**, 2 (2004).
[14] P. Krivosik, N. Mo, S. S. Kalarickal, and C. E. Patton, J. Appl. Phys. **101**, 083901 (2007).
[15] N. Mo, Ph.D. thesis, Colorado State University, 2006.
[16] C. E. Patton and H. J. Van Hook, J. Appl. Phys. **43**, 2872 (1972).
[17] C. E. Patton, Phys. Rev. **179**, 352 (1969).
[18] H. J. Van Hook, J. J. Green, F. Euler, and E. R. Czerlinsky, J. Appl. Phys. **39**, 730 (1968).
[19] N. Mo, Y. Y. Song, and C. E. Patton, J. Appl. Phys. **97**, 093901 (2005).